ELSEVIER

Thin Solid Films 306 (1997) 10–16

thin solid films

# Optical indices of electrochromic tungsten oxide

K. von Rottkay, M. Rubin *, S.-J. Wen

*Lawrence Berkeley National Laboratory, University of California, Berkeley CA 94720, USA*

Received 20 November 1996; accepted 23 April 1997

**Abstract**

Tungsten trioxide ($WO_3$) is the most widely used material for the active layer of electrochromic devices. Knowledge of the complex refractive index over the range of coloration states is required for device design. Optical constants of $WO_3$ over the whole solar spectrum were determined as a function of injected charge. Films of $WO_3$ were prepared by electron-beam evaporation, then colored in several steps by reduction with lithium (Li) up to 68 mC $cm^{-2}$ $\mu m^{-1}$ injected charge. Measurements included variable-angle spectroscopic ellipsometry and spectroscopic transmittance and reflectance at normal incidence. Analysis was complicated by the fact that a transparent-conducting layer of indium tin oxide (ITO) was required to perform lithiation. Optical indices of the glass substrate and ITO transparent conductor were determined separately and then fixed in the model. The indices of $WO_3$ could then be extracted from measurements on the complete structure. A parametric dispersion model corresponding to Gaussian broadening of the oscillators was used to represent the dielectric response of $WO_3$. © 1997 Elsevier Science S.A.

*Keywords:* Electrochromic; Tungsten oxide; Complex refractive index; Colored state

## 1. Introduction

The complex refractive index of electrochromic materials is needed for the design of devices and calculations of system performance. Even for tungsten trioxide ($WO_3$), the most widely used and best studied electrochromic, this information is scattered and incomplete. One of the main deficiencies of existing information is that the range of data tends to be restricted to the visible spectrum, or to a single wavelength. Extrapolation of the extinction coefficient from the near-infrared, where the electrochromic absorption band lies, is not possible with accuracy. Another limitation on existing data is that, at the most, the two extreme coloration states are investigated. A complicating factor is the wide variety of growth techniques and conditions that apparently produce an equally wide variation in materials properties. For large-area applications, the main interest lies in sputtering, chemical vapor deposition and sol–gel techniques.

Villachon-Renard et al. [1] measured transmittance and reflectance data from 250 to 2500 nm of protonated polycrystalline $WO_3$ produced by CVD. They extracted the complex refractive index in the bleached and colored states. Ottermann et al. [2] studied the change in the optical constants of reactively evaporated $WO_3$ in intermediate coloration states as a function of hydrogen content in the range 400–1000 nm. In situ ellipsometric measurements of the protonation process of $WO_3$ deposited by reactive dc-magnetron sputtering are reported by Witham et al. [3]. These data are used to extract the dielectric constants from 310 to 830 nm in the fully bleached and colored state. Bader et al. [4] performed ellipsometry, transmittance and reflectance measurements from 305 to 795 nm on thermally evaporated $WO_3$ intercalated with two different quantities of $Li^+$. They represented highly lithiated $WO_3$ as two separate layers within their optical model due to the dry lithiation process they used. Nagai [5] represented evaporated $WO_3$ colored by lithiation as an effective medium consisting of a mixture between dielectric $WO_3$ and free electron governed $Li_xWO_3$ from 500 to 2000 nm. Recently, using films from the same source as those in this paper, but without an ITO underlayer, Rafla-Yuan et al. [6] determined by ellipsometry the optical indices from 400 to 1000 nm in the two extreme coloration states. An overview of the properties of $WO_3$ including optical properties was recently compiled by Granqvist [7].

In this work, we characterize electron-beam-evaporated $WO_3$ films that are colored by injection of lithium (Li), not only in the extreme bleached and colored states, but also a range of intermediate charge states. The spectral range of

* Corresponding author. Tel.: +1-510-486-7124; fax: +1-510-486-6099; e-mail: mdrubin@lbl.gov.


*PII* S0040-6090(97)00254-X

this study spans the entire solar spectrum from 300 to 2500 nm. We attempt to make the models of structure and dispersion used to analyze the optical data consistent with the physical nature of the materials.

## 2. Experimental

The samples investigated in this paper were deposited by OCLI (Santa Rosa, CA). Glass was first coated with ITO, then with tungsten oxide by e-beam evaporation. The substrates were not heated during deposition. Similar samples were provided by OCLI to participants in the International Energy Agency (IEA) Task 18, which performed electrochemical and optical measurements, as well as various types of structural and compositional analysis. References to this diverse body of work are made throughout this section.

Primary optical measurements were made from 250 to 1000 nm by variable-angle spectroscopic ellipsometry (VASE) using a rotating analyzer instrument (J.A. Woollam). Ellipsometric measurements were taken at 3 angles to obtain adequate sensitivity over the full spectra range. Standard deviations of ellipsometric measurements could be determined experimentally by recording each data point ($\Psi$, $\Delta$) as the average of 30 revolutions of the analyzer. To cover the whole solar spectrum, transmittance and reflectance measurements from 250 to 2500 nm were added. These measurements were taken at near-normal incidence on a Perkin-Elmer Lambda 19 spectrophotometer. The standard deviations of the reflectance and transmittance measurements were not directly measured, but had to be assigned by comparison measurements. They were taken as 0.1% for transmittance and as 0.2% for reflectance data.

Optical measurements were made separately on the ITO layer from a masked-off edge. No optical anisotropy was anticipated or modeled because all $WO_3$ films were found to be amorphous by X-ray diffraction [8].

Thickness was measured by surface profilometry on a Veeco DekTak II A and was subsequently refined by ellipsometry.

Composition of the samples was characterized by Rutherford backscattering spectrometry (RBS) using a 1.95 MeV alpha particle beam in the 165° backscattering geometry.

Electrochromic behavior was examined by inserting Li into the $WO_3$ films in a liquid cell to produce $Li_xW_{1-x}O_3$. The cell consisted of the $WO_3$/ITO working electrode, a lithium counterelectrode and a lithium reference electrode in an electrolytic solution of 1M $LiPF_6$ in propylene carbonate and ethylene carbonate (7:3). The water content of the $LiPF_6$ solution was smaller than 1 ppm. Lithiation was performed in the galvanostatic mode. Therefore, transported charge could be determined by the time during which current was passing the cell. To ensure reversibility of coloration, cyclic voltammetry was performed for 100 cycles between 2.0 and 3.5 V relative to the lithium reference electrode with a scan rate between 1 and 20 mV/s.

AFM measurements were performed with a Park Scientific AutoProbe. Typical scans were taken over $2 \times 2$ $\mu$m at a scan frequency of 1 Hz. A $Si_3N_4$ tip was operated at $F = 5$ nN in contact mode. Whole images were corrected for slope in fast and slow scan directions and analyzed without filtering.

## 3. Optical model

A parametric semiconductor model [9,10] was used to represent the dispersion for $WO_3$. This model corresponds to the case of superposition of many Lorentzian oscillators of slightly different energies. In this case, we obtained a very good fit even when the model parameters were reduced to give a simpler Gaussian form corresponding to strongly inhomogeneous broadening. A single Lorentz oscillator model also gave a good fit over most of the solar spectrum. The main improvement using the Gaussian model was found in the region just above the band gap of $WO_3$, where a Gaussian broadening of the oscillator describes the relatively abrupt absorption edge better than homogeneous Lorentzian broadening [11].

The dispersion model used to fit the data in the colored states comprised one additional oscillator at about 1.3 eV to account for the new absorption band. Since light absorption occurs when an electron absorbs a photon to change from a $WO_3^{5+}$ to a $WO_3^{6+}$, the absorption energy depends on film structure, local surroundings and lattice disorder and can be represented by a two term expression. The first term describes the energy lowering of an electron trapped at $W^{5+}$ site because of lattice polarization. The second takes account of potential energy differences of electrons at nonequivalent $W^{6+}$ sites due to different local surroundings [12]. Those differences increase with lattice distortion as it occurs during $Li^+$ intercalation, therefore leading to a slight blue shift of the absorption band [13], and making it broader.

Ellipsometric and radiometric data were fitted together, weighting both data types according to their standard deviations. The numerical iteration was performed utilizing a Levenberg–Marquardt algorithm until the biased mean square error (MSE) reached its global minimum.

$$\mathrm{MSE} = \frac{1}{N-M}\sum_{\lambda}\left\{\sum_{\Theta}\left[\left(\frac{\Psi_{\Theta,\lambda,\mathrm{cal}} - \Psi_{\Theta,\lambda,\mathrm{exp}}}{\sigma_{\Theta,\lambda,\Psi}}\right)^2 + \left(\frac{\Delta_{\Theta,\lambda,\mathrm{cal}} - \Delta_{\Theta,\lambda,\mathrm{exp}}}{\sigma_{\Theta,\lambda,\Delta}}\right)^2\right] + \left(\frac{T_{\lambda,\mathrm{cal}} - T_{\lambda,\mathrm{exp}}}{\sigma_T}\right)^2 + \left(\frac{R_{\lambda,\mathrm{cal}} - R_{\lambda,\mathrm{exp}}}{\sigma_R}\right)^2\right\}$$

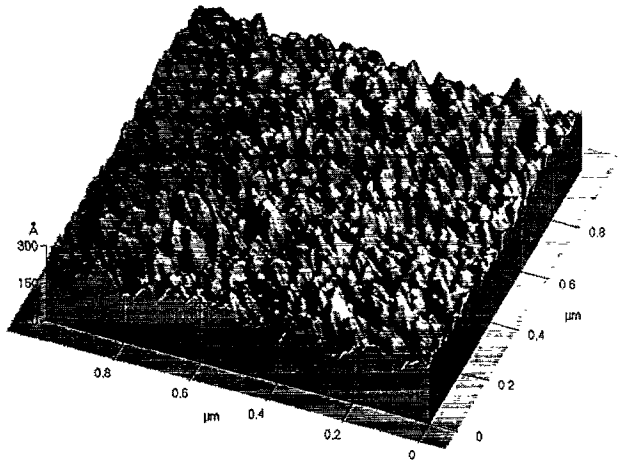


Fig. 1. AFM scan of $WO_3$ surface.

$N$ is the number of total experimental observations, $M$ is the number of fit parameters, $\sigma$ is the standard deviation and the indices $\lambda$ and $\Theta$ are used to sum the data points taken at different wavelengths $\lambda$ and angles $\Theta$. The subscripts 'cal' and 'exp' refer to calculated and experimental values of measurement parameters.

It is necessary to include backside reflections into the model for a semitransparent film if the glass substrate is not roughened, or reflections from the backside are avoided by a different method. We did not roughen the back surface because of the possible need to take subsequent transmittance measurements. Backsurface reflections diminished quickly with increasing injected charge; above the plasma edge of ITO at 1350 nm, the ITO is opaque and obscures the back surface.

## 4. Results

Fig. 1 shows a $1 \times 1$ $\mu$m AFM scan area with magnified ($\times 30$) surface features in the $z$-direction for better visibility. Grain size is estimated to be about 50 nm in rough agreement with other AFM studies on similar films by Chevalier [14] who found average values of 20 nm. Root mean square roughness was calculated to be 2.7 nm for 2 $\mu$m scan length in close agreement to a similar film without an ITO underlayer [6].

Ellipsometric parameters at 61° angle of incidence with the film in the fully bleached state are shown in Fig. 2(a, b). Optical measurements were made at coloration states corresponding to injected volumetric charge densities of 11 mC $cm^{-2}$ $\mu m^{-1}$, 23 mC $cm^{-2}$ $\mu m^{-1}$, 36 mC $cm^{-2}$ $\mu m^{-1}$, 50 mC $cm^{-2}$ $\mu m^{-1}$ and 68 mC $cm^{-2}$ $\mu m^{-1}$. These values were obtained from the areal charge densities determined directly by electrical charge measurements and the thickness of each individual film. We assume that all the injected charge is actually intercalated into the electrochromic film onto optically active sites. This should be a good assumption within safe voltage limits, slow scan rates and charge density below saturation. Film thickness was measured by surface profilometry to be roughly 420 nm in agreement with measurements on similarly deposited films of the same nominal thickness using profilometry [15] and cross-sectional scanning electron microscopy [14], which resulted in values of 420 nm and 360 nm, respectively. The thickness was subsequently refined using ellipsometry as described in the detailed discussion below.

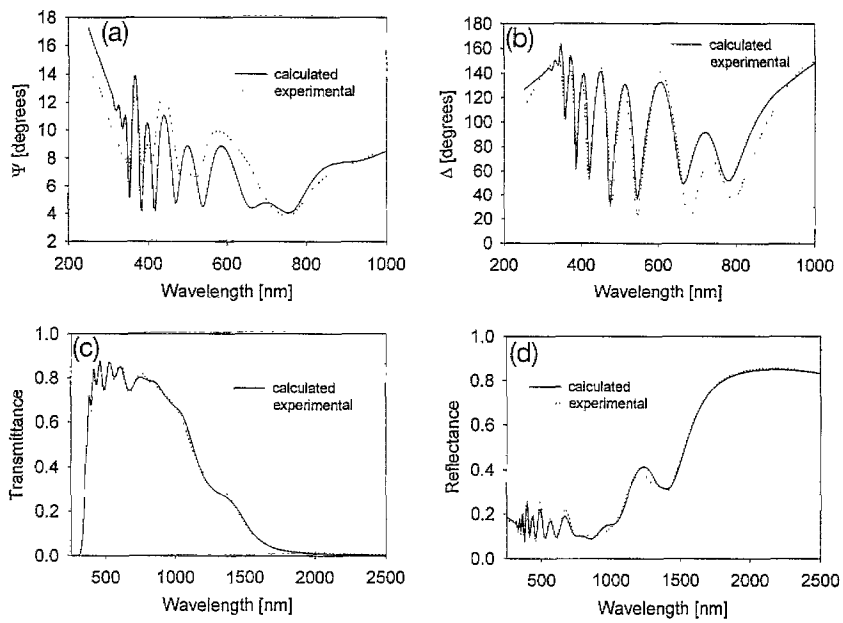


Fig. 2. (a) Spectral ellipsometric $\Psi$ data at 61° angle of incidence of $WO_3$ on ITO-coated glass. (b) Spectral ellipsometric $\Delta$ data at 61° angle of incidence of $WO_3$ on ITO-coated glass. (c) Spectral transmittance data of $WO_3$ on ITO-coated glass. (d) Spectral reflectance data of $WO_3$ on ITO-coated glass.

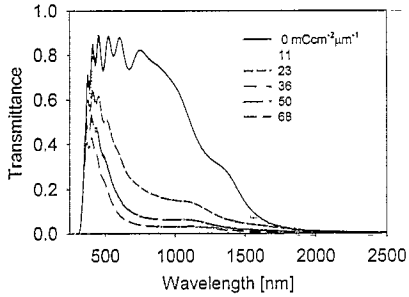


Fig. 3. Spectral transmittance measurements of $WO_3$ on ITO-coated glass in the clear and five different coloration states.

The use of the volumetric charge density as the parameter to normalize for thickness is deliberate; the extinction coefficient of other $WO_3$ films at a given injected charge density should not depend on thickness or mass density. In any case, we find negligible dependence of the real refractive index of $WO_3$ films on thickness over the thickness range of interest for electrochromic applications. This is to be expected a priori despite some apparently contradictory evidence for very thin films in the early stages of nucleation [16] and for materials with unusual variation in structure and porosity with thickness [3].

Nagai et al. used X-ray fluorescence to determine the number density of W atoms and then calculated the mass density of $WO_3$ to be 3.6 g $cm^{-3}$ assuming stoichiometric composition [15]. We found a similar result of 3.65 g $cm^{-3}$ using RBS. This is considerably lower than frequently reported values around 4.9 g $cm^{-3}$. From this additional physical information, the atomic densities of Li represented by the value of $x$ in the chemical formula are $x = 0.06$, $x = 0.11$, $x = 0.18$, $x = 0.25$ and $x = 0.34$. The low density may affect the diffusion coefficient and switching speed, and also the saturation limit, but from the point of view of this optical study, the most relevant effect is an index of refraction slightly lower than average. In some cases, such as for porous sol–gel films, the index may be significantly reduced.

A comparison of transmittance data of $WO_3$ in different colored states (Fig. 3) shows the dramatic changes in its optical behavior with injected charge. Deeply colored samples appear blue due to disproportionately increasing absorption in the red portion of the visible spectrum.

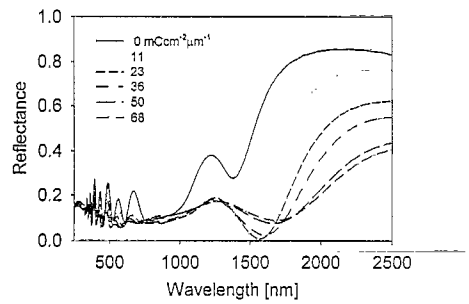


Fig. 4. Spectral reflectance of $WO_3$ on ITO-coated glass in the clear and five different coloration states.

| | |
|---|---|
| ema ($WO_3$ / 50% void) | 4 nm |
| $WO_3$ | 420 nm |
| ITO | 390 nm |
| glass | 1.24 mm |

Fig. 5. Structural model for electron beam evaporated $WO_3$ on ITO-coated glass.

An increase in infrared reflectivity of $WO_3$ with injected charge might be anticipated based on the metallic transformation observed crystalline tungsten bronzes. A strong decrease in reflectivity is observed, however, in the electrochromic half-cell $WO_3$/ITO/glass (Fig. 4). The reflectivity of the $WO_3$ layer itself increases to a small

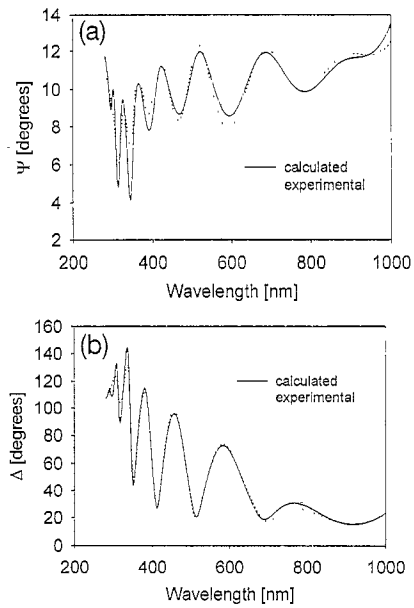


Fig. 6. (a) Spectral ellipsometric $\Psi$ data at 65° angle of incidence of ITO-coated glass. (b) Spectral ellipsometric $\Delta$ data at 65° angle of incidence of ITO-coated glass.

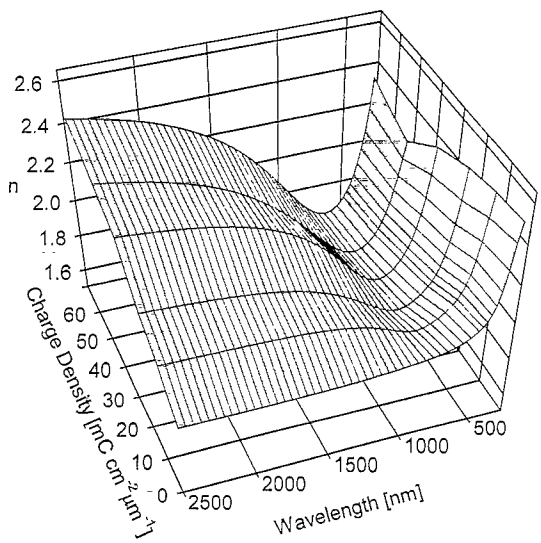


Fig. 7. Real part of the refractive index of $WO_3$ as a function of charge density.

degree in the colored states as shown by the analysis of the optical constants below. Nevertheless, reflectance of the complete system goes down, because polycrystalline or amorphous $WO_3$ has an even greater increase in absorptance, which then masks the fixed high reflectance of the underlying ITO. The interference fringes in the visible also diminish with injected charge as light fails to penetrate to the $WO_3$/ITO interface. In a device, the reflectance above 1400 nm would remain high in any case because light will enter through a transparent conductor.

To analyze this data, we must first define a structural model such as the one depicted in Fig. 5. Both ITO and $WO_3$ are represented by single layers with an additional surface roughness layer on the $WO_3$. Extracting the optical properties of $WO_3$ from this multilayer proved to be difficult; ITO is by itself a very demanding material to properly measure and analyze. When modeling ITO or $WO_3$ alone, a multilayer structural model gives improved fits over single-layer models [17]. Nevertheless, a simplified model of one homogenous ITO layer with one homogenous $WO_3$ layer (Fig. 5) was chosen to represent the entire sample structure instead of using the optimum models found for either film alone. This minimizes the correlation of fit parameters with errors in information about the

Table 1
Spectral optical constants with 90% confidence limits of electron-beam-evaporated $WO_3$ in the clear and two colored states characterized by injected charge density

| λ (nm) | Clear state | | | | 11 mC cm$^{-2}$ μm$^{-1}$ | | | | 23 mC cm$^{-2}$ μm$^{-1}$ | | | |
|---|---|---|---|---|---|---|---|---|---|---|---|---|
| | $n$ | ± | $\kappa$ | ± | $n$ | ± | $\kappa$ | ± | $n$ | ± | $\kappa$ | ± |
| 300 | 2.52 | 0.01 | 0.34 | 0.004 | 2.50 | 0.01 | 0.25 | 0.003 | 2.47 | 0.05 | 0.22 | 0.001 |
| 325 | 2.42 | 0.01 | 0.15 | 0.001 | 2.38 | 0.01 | 0.11 | 0.000 | 2.31 | 0.04 | 0.10 | 0.001 |
| 350 | 2.29 | 0.01 | 0.04 | 0.001 | 2.27 | 0.02 | 0.04 | 0.001 | 2.19 | 0.03 | 0.05 | 0.001 |
| 375 | 2.19 | 0.02 | 0.01 | 0.001 | 2.17 | 0.02 | 0.02 | 0.001 | 2.10 | 0.03 | 0.02 | 0.001 |
| 400 | 2.12 | 0.02 | 0.00 | 0.000 | 2.10 | 0.02 | 0.01 | 0.001 | 2.03 | 0.03 | 0.02 | 0.001 |
| 425 | 2.07 | 0.02 | 0.00 | 0.000 | 2.05 | 0.02 | 0.01 | 0.000 | 1.98 | 0.03 | 0.02 | 0.001 |
| 450 | 2.04 | 0.02 | 0.00 | 0.000 | 2.01 | 0.02 | 0.01 | 0.000 | 1.94 | 0.03 | 0.02 | 0.001 |
| 475 | 2.02 | 0.02 | 0.00 | 0.000 | 1.98 | 0.02 | 0.02 | 0.000 | 1.91 | 0.03 | 0.03 | 0.001 |
| 500 | 2.00 | 0.02 | 0.00 | 0.000 | 1.96 | 0.02 | 0.02 | 0.000 | 1.88 | 0.03 | 0.04 | 0.001 |
| 550 | 1.97 | 0.02 | 0.00 | 0.000 | 1.93 | 0.02 | 0.03 | 0.000 | 1.85 | 0.03 | 0.06 | 0.001 |
| 600 | 1.95 | 0.02 | 0.00 | 0.000 | 1.90 | 0.02 | 0.05 | 0.001 | 1.82 | 0.03 | 0.09 | 0.001 |
| 650 | 1.94 | 0.02 | 0.00 | 0.000 | 1.88 | 0.02 | 0.06 | 0.002 | 1.80 | 0.03 | 0.12 | 0.001 |
| 700 | 1.93 | 0.02 | 0.00 | 0.000 | 1.87 | 0.02 | 0.08 | 0.002 | 1.79 | 0.03 | 0.15 | 0.001 |
| 750 | 1.92 | 0.02 | 0.00 | 0.000 | 1.86 | 0.02 | 0.10 | 0.002 | 1.79 | 0.03 | 0.18 | 0.001 |
| 800 | 1.91 | 0.02 | 0.00 | 0.000 | 1.86 | 0.02 | 0.12 | 0.001 | 1.80 | 0.03 | 0.21 | 0.001 |
| 850 | 1.91 | 0.02 | 0.00 | 0.000 | 1.88 | 0.02 | 0.14 | 0.000 | 1.82 | 0.03 | 0.24 | 0.001 |
| 900 | 1.90 | 0.02 | 0.00 | 0.000 | 1.89 | 0.02 | 0.15 | 0.001 | 1.84 | 0.03 | 0.25 | 0.001 |
| 950 | 1.90 | 0.02 | 0.00 | 0.000 | 1.91 | 0.02 | 0.16 | 0.001 | 1.87 | 0.03 | 0.27 | 0.001 |
| 1000 | 1.90 | 0.02 | 0.00 | 0.000 | 1.92 | 0.02 | 0.16 | 0.002 | 1.89 | 0.03 | 0.27 | 0.001 |
| 1050 | 1.90 | 0.02 | 0.00 | 0.000 | 1.93 | 0.02 | 0.16 | 0.002 | 1.91 | 0.03 | 0.28 | 0.001 |
| 1100 | 1.89 | 0.02 | 0.00 | 0.000 | 1.94 | 0.02 | 0.15 | 0.001 | 1.93 | 0.03 | 0.28 | 0.001 |
| 1150 | 1.89 | 0.02 | 0.00 | 0.000 | 1.95 | 0.02 | 0.15 | 0.001 | 1.95 | 0.03 | 0.27 | 0.001 |
| 1200 | 1.89 | 0.02 | 0.00 | 0.000 | 1.96 | 0.02 | 0.14 | 0.001 | 1.97 | 0.03 | 0.27 | 0.001 |
| 1250 | 1.89 | 0.02 | 0.00 | 0.000 | 1.97 | 0.02 | 0.14 | 0.001 | 1.98 | 0.03 | 0.27 | 0.001 |
| 1300 | 1.89 | 0.02 | 0.00 | 0.000 | 1.97 | 0.02 | 0.14 | 0.001 | 1.99 | 0.03 | 0.26 | 0.001 |
| 1350 | 1.89 | 0.02 | 0.00 | 0.000 | 1.98 | 0.02 | 0.13 | 0.001 | 2.00 | 0.03 | 0.25 | 0.001 |
| 1400 | 1.88 | 0.02 | 0.00 | 0.000 | 1.98 | 0.02 | 0.13 | 0.001 | 2.01 | 0.03 | 0.25 | 0.001 |
| 1450 | 1.88 | 0.02 | 0.00 | 0.000 | 1.98 | 0.02 | 0.12 | 0.001 | 2.02 | 0.03 | 0.24 | 0.001 |
| 1500 | 1.88 | 0.02 | 0.00 | 0.000 | 1.99 | 0.02 | 0.12 | 0.001 | 2.03 | 0.03 | 0.23 | 0.001 |
| 1550 | 1.88 | 0.02 | 0.00 | 0.000 | 1.99 | 0.02 | 0.11 | 0.001 | 2.04 | 0.03 | 0.23 | 0.001 |
| 1600 | 1.88 | 0.02 | 0.00 | 0.000 | 1.99 | 0.02 | 0.11 | 0.001 | 2.05 | 0.03 | 0.22 | 0.001 |
| 1650 | 1.88 | 0.02 | 0.00 | 0.000 | 1.99 | 0.02 | 0.11 | 0.001 | 2.05 | 0.03 | 0.22 | 0.001 |
| 1700 | 1.88 | 0.02 | 0.00 | 0.000 | 1.99 | 0.02 | 0.10 | 0.001 | 2.06 | 0.03 | 0.21 | 0.001 |
| 1750 | 1.88 | 0.02 | 0.00 | 0.000 | 2.00 | 0.02 | 0.10 | 0.001 | 2.06 | 0.03 | 0.21 | 0.001 |
| 1800 | 1.88 | 0.02 | 0.00 | 0.000 | 2.00 | 0.02 | 0.10 | 0.001 | 2.07 | 0.02 | 0.20 | 0.001 |
| 1850 | 1.88 | 0.02 | 0.00 | 0.000 | 2.00 | 0.02 | 0.10 | 0.001 | 2.07 | 0.02 | 0.20 | 0.001 |
| 1900 | 1.88 | 0.02 | 0.00 | 0.000 | 2.00 | 0.02 | 0.09 | 0.001 | 2.07 | 0.02 | 0.19 | 0.001 |
| 1950 | 1.88 | 0.02 | 0.00 | 0.000 | 2.00 | 0.02 | 0.09 | 0.000 | 2.08 | 0.02 | 0.19 | 0.001 |
| 2000 | 1.88 | 0.02 | 0.00 | 0.000 | 2.00 | 0.02 | 0.09 | 0.000 | 2.08 | 0.02 | 0.18 | 0.001 |
| 2100 | 1.88 | 0.02 | 0.00 | 0.000 | 2.00 | 0.02 | 0.08 | 0.000 | 2.08 | 0.02 | 0.17 | 0.001 |
| 2200 | 1.88 | 0.02 | 0.00 | 0.000 | 2.00 | 0.02 | 0.08 | 0.000 | 2.09 | 0.02 | 0.17 | 0.001 |
| 2300 | 1.88 | 0.02 | 0.00 | 0.000 | 2.01 | 0.02 | 0.08 | 0.000 | 2.09 | 0.02 | 0.16 | 0.001 |
| 2400 | 1.88 | 0.02 | 0.00 | 0.000 | 2.01 | 0.02 | 0.07 | 0.000 | 2.10 | 0.02 | 0.15 | 0.001 |
| 2500 | 1.88 | 0.02 | 0.00 | 0.000 | 2.01 | 0.02 | 0.07 | 0.000 | 2.10 | 0.02 | 0.15 | 0.001 |

rest of the stack, but the resultant fit of ellipsometric data is relatively poor (Fig. 2(a, b)). The representation of spectrophotometric data by the same fit parameters, however, is better (Fig. 2(c, d)). This indicates that the obtained optical constants adequately represent the average properties of the thin films, whereas the reduced complexity of the structural model does not account for imperfections as interface roughness or a gradient in the refractive index [17].

The complex refractive index of the ITO was taken from a masked-off spot on the given film rather than from a supposedly representative sample. Even so, it is possible that these optical constants do not closely represent the part of the ITO on which the $WO_3$ was deposited; some oxidation is likely to occur during the initial evaporation of $WO_3$. Comparing fits on ellipsometric data of the ITO-coated glass substrate (Fig. 6(a, b)) with Fig. 2(a, b) clearly shows a clear decrease in fit quality, although the dispersion of clear $WO_3$ is much easier to model than that of ITO. The fit could be improved if one fitted only for the optical constants of the buried ITO layer while leaving all other parameters fixed. In this case, the uncertainties of the fit parameters are pretty large. Bruggeman effective medium analysis of ellipsometric data on ITO yielded a surface roughness of 4.3 nm [18]. In the model for the whole electrochromic half cell including $WO_3$, however,

Table 2
Spectral optical constants with confidence limits of electron beam evaporated $WO_3$ in three colored states characterized by injected charge density

| λ (nm) | 36 mC $cm^{-2}$ $\mu m^{-1}$ | | | | 50mC $cm^{-2}\mu m^{-1}$ | | | | 68 mC $cm^{-2}$ $\mu m^{-1}$ | | | |
|---|---|---|---|---|---|---|---|---|---|---|---|---|
| | $n$ | ± | $\kappa$ | ± | $n$ | ± | $\kappa$ | ± | $n$ | ± | $\kappa$ | ± |
| 300 | 2.39 | 0.020 | 0.24 | 0.006 | 2.24 | 0.030 | 0.27 | 0.004 | 2.35 | 0.020 | 0.20 | 0.000 |
| 325 | 2.26 | 0.020 | 0.12 | 0.002 | 2.16 | 0.020 | 0.16 | 0.001 | 2.20 | 0.020 | 0.10 | 0.002 |
| 350 | 2.14 | 0.020 | 0.06 | 0.001 | 2.07 | 0.020 | 0.09 | 0.000 | 2.08 | 0.010 | 0.06 | 0.002 |
| 375 | 2.05 | 0.010 | 0.04 | 0.002 | 2.00 | 0.010 | 0.06 | 0.000 | 1.98 | 0.010 | 0.04 | 0.002 |
| 400 | 1.98 | 0.010 | 0.03 | 0.002 | 1.93 | 0.010 | 0.05 | 0.000 | 1.91 | 0.010 | 0.05 | 0.001 |
| 425 | 1.93 | 0.010 | 0.04 | 0.001 | 1.88 | 0.010 | 0.05 | 0.000 | 1.85 | 0.010 | 0.06 | 0.000 |
| 450 | 1.88 | 0.010 | 0.05 | 0.001 | 1.83 | 0.010 | 0.06 | 0.000 | 1.80 | 0.010 | 0.08 | 0.001 |
| 475 | 1.85 | 0.010 | 0.07 | 0.001 | 1.80 | 0.010 | 0.08 | 0.000 | 1.76 | 0.010 | 0.10 | 0.001 |
| 500 | 1.82 | 0.010 | 0.09 | 0.000 | 1.77 | 0.010 | 0.10 | 0.001 | 1.73 | 0.010 | 0.13 | 0.002 |
| 550 | 1.78 | 0.010 | 0.13 | 0.000 | 1.73 | 0.010 | 0.14 | 0.001 | 1.69 | 0.010 | 0.19 | 0.004 |
| 600 | 1.75 | 0.010 | 0.17 | 0.000 | 1.70 | 0.010 | 0.20 | 0.002 | 1.67 | 0.010 | 0.25 | 0.006 |
| 650 | 1.74 | 0.010 | 0.22 | 0.001 | 1.69 | 0.010 | 0.25 | 0.003 | 1.66 | 0.010 | 0.31 | 0.008 |
| 700 | 1.74 | 0.010 | 0.28 | 0.001 | 1.70 | 0.010 | 0.30 | 0.003 | 1.67 | 0.010 | 0.37 | 0.011 |
| 750 | 1.76 | 0.010 | 0.32 | 0.002 | 1.71 | 0.010 | 0.35 | 0.004 | 1.69 | 0.010 | 0.43 | 0.014 |
| 800 | 1.79 | 0.010 | 0.36 | 0.001 | 1.73 | 0.010 | 0.39 | 0.003 | 1.72 | 0.010 | 0.48 | 0.016 |
| 850 | 1.82 | 0.010 | 0.40 | 0.000 | 1.76 | 0.010 | 0.43 | 0.002 | 1.75 | 0.010 | 0.52 | 0.017 |
| 900 | 1.86 | 0.010 | 0.42 | 0.001 | 1.80 | 0.010 | 0.46 | 0.002 | 1.79 | 0.010 | 0.56 | 0.017 |
| 950 | 1.90 | 0.010 | 0.43 | 0.001 | 1.83 | 0.020 | 0.49 | 0.001 | 1.84 | 0.010 | 0.58 | 0.017 |
| 1000 | 1.93 | 0.010 | 0.44 | 0.002 | 1.87 | 0.020 | 0.50 | 0.000 | 1.88 | 0.020 | 0.60 | 0.016 |
| 1050 | 1.97 | 0.010 | 0.45 | 0.003 | 1.90 | 0.020 | 0.52 | 0.000 | 1.92 | 0.020 | 0.61 | 0.015 |
| 1100 | 2.00 | 0.010 | 0.45 | 0.003 | 1.94 | 0.020 | 0.53 | 0.001 | 1.96 | 0.020 | 0.62 | 0.014 |
| 1150 | 2.02 | 0.010 | 0.44 | 0.003 | 1.97 | 0.020 | 0.53 | 0.001 | 2.00 | 0.020 | 0.63 | 0.013 |
| 1200 | 2.05 | 0.010 | 0.44 | 0.003 | 2.00 | 0.020 | 0.53 | 0.001 | 2.03 | 0.020 | 0.63 | 0.012 |
| 1250 | 2.07 | 0.010 | 0.43 | 0.003 | 2.03 | 0.020 | 0.53 | 0.002 | 2.07 | 0.020 | 0.63 | 0.011 |
| 1300 | 2.10 | 0.010 | 0.42 | 0.003 | 2.06 | 0.030 | 0.53 | 0.002 | 2.10 | 0.020 | 0.62 | 0.010 |
| 1350 | 2.11 | 0.010 | 0.41 | 0.003 | 2.09 | 0.030 | 0.53 | 0.002 | 2.13 | 0.020 | 0.62 | 0.009 |
| 1400 | 2.13 | 0.010 | 0.40 | 0.003 | 2.11 | 0.030 | 0.52 | 0.002 | 2.15 | 0.020 | 0.61 | 0.008 |
| 1450 | 2.15 | 0.010 | 0.39 | 0.003 | 2.13 | 0.030 | 0.51 | 0.002 | 2.18 | 0.020 | 0.61 | 0.007 |
| 1500 | 2.16 | 0.010 | 0.39 | 0.003 | 2.15 | 0.030 | 0.51 | 0.002 | 2.20 | 0.020 | 0.60 | 0.007 |
| 1550 | 2.17 | 0.010 | 0.38 | 0.003 | 2.17 | 0.030 | 0.50 | 0.002 | 2.22 | 0.020 | 0.59 | 0.006 |
| 1600 | 2.18 | 0.010 | 0.37 | 0.003 | 2.19 | 0.030 | 0.49 | 0.002 | 2.24 | 0.020 | 0.58 | 0.005 |
| 1650 | 2.19 | 0.010 | 0.36 | 0.003 | 2.20 | 0.030 | 0.49 | 0.002 | 2.26 | 0.020 | 0.57 | 0.005 |
| 1700 | 2.20 | 0.010 | 0.35 | 0.003 | 2.22 | 0.030 | 0.48 | 0.002 | 2.28 | 0.020 | 0.56 | 0.004 |
| 1750 | 2.21 | 0.010 | 0.34 | 0.003 | 2.23 | 0.030 | 0.47 | 0.002 | 2.30 | 0.020 | 0.56 | 0.004 |
| 1800 | 2.22 | 0.010 | 0.33 | 0.002 | 2.24 | 0.020 | 0.46 | 0.002 | 2.31 | 0.020 | 0.55 | 0.004 |
| 1850 | 2.23 | 0.010 | 0.33 | 0.002 | 2.26 | 0.020 | 0.45 | 0.002 | 2.32 | 0.020 | 0.54 | 0.003 |
| 1900 | 2.23 | 0.010 | 0.32 | 0.002 | 2.27 | 0.020 | 0.45 | 0.002 | 2.34 | 0.020 | 0.53 | 0.003 |
| 1950 | 2.24 | 0.010 | 0.31 | 0.002 | 2.28 | 0.020 | 0.44 | 0.002 | 2.35 | 0.020 | 0.52 | 0.003 |
| 2000 | 2.24 | 0.010 | 0.30 | 0.002 | 2.29 | 0.020 | 0.43 | 0.002 | 2.36 | 0.020 | 0.51 | 0.002 |
| 2100 | 2.25 | 0.010 | 0.29 | 0.002 | 2.31 | 0.020 | 0.42 | 0.002 | 2.38 | 0.020 | 0.49 | 0.002 |
| 2200 | 2.26 | 0.010 | 0.28 | 0.002 | 2.32 | 0.020 | 0.40 | 0.001 | 2.40 | 0.020 | 0.48 | 0.002 |
| 2300 | 2.27 | 0.010 | 0.27 | 0.002 | 2.33 | 0.020 | 0.39 | 0.001 | 2.42 | 0.020 | 0.46 | 0.001 |
| 2400 | 2.28 | 0.010 | 0.26 | 0.002 | 2.35 | 0.020 | 0.38 | 0.001 | 2.43 | 0.020 | 0.45 | 0.001 |
| 2500 | 2.28 | 0.010 | 0.25 | 0.002 | 2.36 | 0.020 | 0.36 | 0.001 | 2.44 | 0.020 | 0.43 | 0.001 |

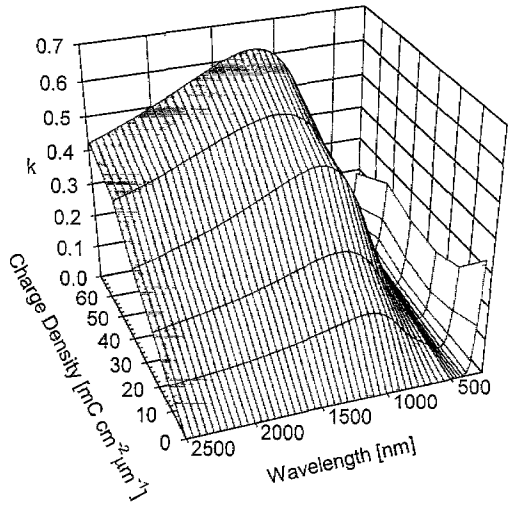


Fig. 8. Extinction coefficient $\kappa$ for $WO_3$ as a function of charge density.

the fit parameters did not show any sensitivity to interface roughness.

The complex refractive index $(n - i\kappa)$ was determined from 300 to 2500 nm as a function of intercalated charge density (Figs. 7 and 8). For ease of use, optical indices at selected wavelengths are also given in Tables 1 and 2. The 90% confidence limits refer to random measurement errors and uncertainty of fits. A major source for errors, however, are systematic errors in experimental setup and sample condition, as well as systematic differences between experimental data and fits [19]. Therefore, these confidence limits should better be interpreted carefully as precision indicator at the respective wavelength and injected charge level. For the clear state, these values are in close agreement with optical indices determined for similar films [6] from 400 to 1000 nm without an ITO underlayer. The optical indices of those films when colored by proton injection show a similar shape when compared to the highest levels of charge density in this paper. The protonated films, however, were colored by application of a local potential and injected charge could not be determined, so the oscillator strengths may not be equal.

## 5. Conclusion

Using a combination of ellipsometry and spectrophotometry, it was possible to extract the optical indices of e-beam evaporated $WO_3$ from measurements on a structure that includes surface roughness and buried ITO conductor. Including the conductor layer in the stack allowed the film to be electrochemically reduced with Li, so that a full set of properties could be determined in several intermediate charge states. It was also possible to determine the optical indices of $WO_3$ over the entire solar spectrum despite the opacity of the ITO conductor in part of the infrared. This data is then suitable to model and design the operation of electrochromic devices for visual and solar applications such as windows for buildings and vehicles.

## Acknowledgements

The films studied in this work were kindly provided by Optical Coating Laboratories in Santa Rosa, CA. This work was supported by the Assistant Secretary for Energy Efficiency and Renewable Energy, Office of Building Technologies, Building Systems and Materials Division of the US Department of Energy under Contract No. DE-AC03-76SF00098.

## References

[1] Y. Villachon-Renard, G. Leveque, A. Abdellaoui, A. Donnadieu, Thin Solid Films 203 (1991) 33.
[2] C. Ottermann, A. Temmink, K. Bange, SPIE 1272 (1990) 111.
[3] H.S. Witham, P. Chindaudom, I. An, R.W. Collins, R. Messier, K. Vedam, J. Vac. Sci. Technol. A 11 (4) (1993) 1881.
[4] G. Bader, P.V. Ashrit, V.-V. Truong, SPIE 2531 (1995) 70.
[5] J. Nagai, SPIE 1016 (1988) 28.
[6] H. Rafla-Yuan, J.G.H. Mathew, B.P. Hichwa, J. Electrochem. Soc. 143 (1996) 2341.
[7] C.G. Granqvist, Handbook of Inorganic Electrochromic Materials, Elsevier, Amsterdam, 1995, p. 17.
[8] K. Yoshimura, IEA Report T18/B3/JP/95 (June 1995).
[9] C. Herzinger, B. Johs, Guide to Using WVASE32™, J.A. Woollam Lincoln, NE, 1996, p. 347.
[10] C.C. Kim, J.W. Garland, H. Abad, P.M. Raccah, Phys. Rev. B 45 (1992) 11749.
[11] X.-F. He, J. Opt. Soc. Am. B 14 (1997) 17.
[12] I.V. Shiyanovskaya, J. Non-Cryst. Sol. 187 (1995) 420.
[13] A. Nakamura, S. Yamada, Appl. Phys. 24 (1981) 55.
[14] B. Chevalier, IEA Report T18/B3/FRA1/95 (January 1995).
[15] J. Nagai, G.D. McMeeking, Y. Noutomi, IEA Report T18/b3/JPN1/95.
[16] S. Sacre, L.K. Thomas, Thin Solid Films 203 (1991) 221.
[17] K. von Rottkay, M. Rubin, N. Ozer, Mater. Res. Soc. Symp. Proc. 403 (1996) 551.
[18] D.E. Aspnes, J.B. Theeten, F. Hottier, Phys. Rev. B 20 (1979) 3292.
[19] G.E. Jellison Jr., Thin Solid Films 234 (1993) 416.